Predicting the Young's modulus of nanowires from first-principles calculations on their surface and bulk materials

Guofeng Wang [1,*] and Xiaodong Li [2]

[1] Department of Mechanical Engineering, Indiana University-Purdue University Indianapolis, Indianapolis, IN 46202

[2] Department of Mechanical Engineering, University of South Carolina, Columbia, SC 29208

Abstract:

Using the concept of surface stress, we developed a model that is able to predict the Young's modulus of nanowires as a function of nanowire diameters from the calculated properties of their surface and bulk materials. We took both equilibrium strain effect and surface stress effect into consideration to account for the geometric size influence on the elastic properties of nanowires. In this work, we combined first-principles density functional theory calculations of material properties with linear elasticity theory of clamped-end three-point bending. Furthermore, we applied this computation approach to Ag, Au, and ZnO nanowires. For both Ag and Au nanowires, our theoretical predictions agree well with the experimental data in the literature. For ZnO nanowires, our predictions are qualitatively consistent with some of experimental data for ZnO nanostructures. Consequently, we found that surface stress plays a very important role in determining the Young's modulus of nanowires. Our finding suggests that the elastic properties of nanowires could be possibly engineered by altering the surface stress of their lateral surfaces.

[*] Corresponding author. Electronic mail: wang83@iupui.edu

I. INTRODUCTION

Currently, many powerful electromechanical devices can be designed and fabricated at the micro level such as microelectromechanical systems (MEMS). It is a highly active research forefront to develop future electromechanical devices with size in the nano scale, for instance, nanoelectromechanical systems (NEMS). [1] For example, a nanogenerator, which uses ZnO nanowires to convert mechanical energy to electrical energy, has been successfully fabicated.[2] NEMS employs one-dimensional (1D) nanomaterials (nanowires, nanobelts, and/or nanotubes) as its active components to generate, transmit, and convert powers and motions. Hence, the dependence of the mechanical properties on the geometric size of 1D nanomaterials is a very important factor in affecting the performance of those 1D nanomaterials in the NEMS devices. So far, several different fashions of the size dependence of the elastic properties of nanomaterials have been revealed: (1) Young's modulus increases with the decreasing size, for example, in Ag and Pd nanowires; [3,4] (2) Young's modulus decreases with the decreasing size, for example, in Cr and Si nanocantilevers; [5,6] and (3) Young's modulus shows little dependence of the size of the nanomaterials such as Au nanowires.[7] Moreover, for a same nanomaterial, different research groups could observe and report the opposite size-dependence of its elastic properties. For the case of 1D ZnO nanomaterials, some measurements [8-13] indicated that their Young's modulus should be lower than the bulk modulus. In contrast, some investigations [14,15] declared the observation of the exact opposite trend.

Despite of its significance, the mechanism for how the Young's modulus of 1D nanomaterials depends on their size and surface conditions is barely understood.

Generally speaking, the surface of the nanomaterials will exert great influence on its overall mechanical properties. Consequently, the Young's modulus of a 1D nanomaterial is believed to be determined by both bulk elastic modulus and surface elastic modulus.[16,17] In other words, the elastic response of a 1D nanomaterial depends strongly on its surface elastic constant.[18] The relative increase or decrease of the elastic properties of nanomaterials may be the results of surface bonding [19] and bulk nonlinear phenomena.[20] Therefore, it is of great interest to quantitatively investigate how to predict the elastic properties of 1D nanomaterials from the properties of the surface and bulk materials. In this paper, we will present a model developed for that purpose.

Our model mainly focuses on the role of surface stress effect in determining the Young's modulus of 1D nanomaterials. Surface stress is defined as the reversible work per unit area required to elastically stretch a surface.[21] The experimental data and analysis in Ref. 3 showed that a positive (tensile) surface stress will lead to an increase in Young's modulus as the diameter decreases. Our previous theoretical study pointed out that a negative (compressive) surface stress is the reason for the observed decrease in Young's modulus with decreasing diameter of the ZnO nanowires. [22] Recently, it was proposed that the surface stress effect are also responsible for the reduction in the resonant frequencies of fixed/fixed Si nanowires [23] and the asymmetric yield strength of Al nanowires. [24] Here, we further elucidate how the surface stress affects the Young's modulus of nanowires.

This paper is structured as follows: in Sec. II, we present our model that predicts the Young's modulus of the nanowire with a given diameter based on surface stress effect; in Sec. III, we give the required properties of bulk and surface materials calculated using

3

first-principles density functional theory (DFT) method and then evaluate the Young's modulus of the nanowires using our developed model. Our model predictions are compared with the available experimental data in this section; at last, final conclusions are drawn in Sec. IV.

II. MODELS

In this work, we derived the quantitative relation between the Young's modulus of a nanowire (with a circular cross-section) and its material properties assuming clamped-end three-point bending loading condition.

The total energy of such nanowire is expressed as the sum of the energy contributions from bulk and surface materials. We assumed the external surface of nanowires is a surface layer with a thickness of t.

$$U = \frac{\pi(D-2t)^2}{4}L\Omega(\varepsilon) + \pi DL\gamma(\varepsilon) \tag{1}$$

where, $\Omega(\varepsilon)$ is the bulk energy density in the nanowire core, $\gamma(\varepsilon)$ is the surface energy of the nanowire surfaces, D is the diameter of the nanowire, and L is the length of the nanowire.

A. Effect of equilibrium strain

The equilibrium bulk material has the lowest energy at the zero-strain state of the crystal lattices. However, the lowest-energy configuration of the surface layers does not necessary have the same lattice parameters as the zero-strain state of the bulk materials. This is because the arrangement and separation of atoms are different in the surface and

4

in the bulk crystal. Hence, the bulk energy density $\Omega(\varepsilon)$ and the surface energy $\gamma(\varepsilon)$ can be written in the following forms.

$$\Omega(\varepsilon) = \Omega_{min} + \frac{1}{2} K_b \varepsilon^2 \tag{2a}$$

$$\gamma(\varepsilon) = \gamma_{min} + \frac{1}{2} K_s \left(\varepsilon - \varepsilon_0^S \right)^2 \tag{2b}$$

Where, K_b is the bulk elastic modulus, K_s is related to the elastic modulus of infinitely large extended surface, and ε_0^S is the strain at which the surface energy reaches its minimum. Ω_{min} and γ_{min} are the minimal bulk energy density and the minimal surface energy, respectively.

Thus, we could determine the equilibrium strain (ε^*) in the nanowire through $\frac{\partial U}{\partial \varepsilon}(\varepsilon^*) = 0$ by considering Eqs. (1) and (2).

$$\varepsilon^* = \frac{K_s \cdot \varepsilon_0^S}{\frac{(D-2t)^2}{4D} K_b + K_s} \tag{3}$$

The existence of this equilibrium strain in the nanowires has already been revealed in previous molecular dynamics simulations. [25,26] The equilibrium strain would affect the elastic modulus of the core (bulk) region of the nanowires.

If a nanowire is deformed by a strain δ from its equilibrium state (with an equilibrium strain ε^*) under a load, then $\delta = \frac{\varepsilon}{\left(1 + \varepsilon^*\right)}$ (note: ε is the strain with respect to the equilibrium crystal lattice).

Hence, the Young's modulus contributed from the nanowire's core should be:

$$E_{core} = \frac{\partial^2 \Omega(\varepsilon)}{\partial \delta^2} = \left(1 + \varepsilon^*\right)^2 E_b \qquad (4)$$

B. Effect of surface stress

Surface stress ($g = \gamma + \frac{\partial \gamma}{\partial \varepsilon}$) is the reversible work per unit area required to elastically stretch a surface. [21] When a circular nanowire is subject to a deformation, its total surface area will change by $\pi D(1-v)\Delta L$ (v is the Poisson's ratio). Consequently, the energy change associated with the surface deformation of the nanowire is $\Delta U_S = \pi D(1-v)g\Delta L$. It is noted that the change of nanowire length (ΔL) is dependent upon the loading conditions: for axial tensile loading, ΔL is linearly proportional to the strain; in contrast, ΔL is proportional to the square of the deflection under clamped-end three-point bending.

Clamped-end three-point bending test is most often used to measure the Young's modulus of nanostructures. [4,7,11] In this work, we derive our model just for this loading condition. When a concentrated load P acts at the middle point of a nanowire with a length of L and fixed on both ends, the elastic deflection curve of the nanowire would be as follows. [27]

$$y(x) = \frac{Px^2}{48EI}(3L - 4x) \qquad \left(0 \le x \le \frac{L}{2}\right) \qquad (5)$$

For the nanowire with a circular cross-section, moment of inertia $I = \frac{\pi D^4}{64}$. Thus, the maximum deflection is $d = \frac{PL^3}{192EI}$ occurring at $x=L/2$. In experimental tests, the Young's modulus of the nanowire is determined by $E = \left(\frac{P}{d}\right)\left(\frac{L^3}{192I}\right)$.

The elongation of the nanowire under bending is given by

$$\Delta L = \int_0^{L/2} [y'(x)]^2 \, dx = \frac{12}{5} \frac{d^2}{L} \tag{6}$$

Consequently, the resistant force to the bending due to surface stress in the nanowire is

$$P_S = -\frac{\partial U_S}{\partial d} = -\frac{24}{5} \pi D (1-\nu) g \frac{d}{L} \tag{7}$$

Hence, the Young's modulus contributed from the nanowire's surface should be:

$$E_{surface} = \left(\frac{-P_S}{d}\right)\left(\frac{L^3}{192I}\right) = \frac{8}{5} g(1-\nu)\frac{L^2}{D^3} \tag{8}$$

Similar derivation has been done previously by Cuenot et al. [3] Note that $E_{surface}$ in Eq. (8) is the Young's modulus of the curved circular nanowire surface, different from K_s in Eqs. (2b) and (3) referring to the elastic modulus of the flat extended surface along a specific crystalline direction.

C. Young's modulus of nanowire

Combining Eq. (4) and Eq. (8), we express the Young's modulus of nanowires, which have circular cross-sections and are subject to clamped-end three-point bending, as the following function.

$$E_{nanowire} = (1+\varepsilon^*)^2 E_b + \frac{8}{5} g(1-\nu)\frac{L^2}{D^3} \tag{9}$$

With the increase of the diameter (D) of the nanowires, the equilibrium strain ε^* would approach to zero according to Eq. (3). Therefore, $E_{nanowire}$ in Eq. (9) would be equal to bulk Young's modulus E_b when D reaches the limit of bulk materials.

III. RESULTS

In order to examine the reliability of Eq. (9), we performed first-principles calculations on example materials Ag, Au, and ZnO, predicted their size-dependent Young's modulus based on Eq. (9) using the calculated theoretical data, and further compared our predictions with experimental measurements. Our first-principles calculations for the three materials were performed using the VASP code. [28,29] We used the projector augmented wave method [30] and the generalized gradient approximation of Perdew and Wang [31] for exchange and correlation. We chose a kinetic energy cutoff of 600 eV to expand the electronic wave functions in the plane wave basis. The energy convergence for all geometry optimization was set to be 1×10^{-5} eV.

A. Bulk materials

For Ag, Au, and ZnO in their bulk states, we computed the equilibrium lattice constants and the corresponding elastic constants using first-principles calculations. The results are given in Tables I and II. The equilibrium Ag and Au crystals have faced-centered cubic (fcc) structures, while equilibrium ZnO has a wurtzite crystal structure. Through calculations, we are able to determine the lattice constants that lead to the minimal energy of the respective crystal structures. Using $16 \times 16 \times 16$ k-point grid for k-space integration, we determined the elastic constants of the crystals following the procedure given in Ref. 32 (for fcc Ag and Au) and Ref. 33 (for wurtzite ZnO). As shown in Tables I and II, our theoretical predictions agree well with the corresponding experimental data. Furthermore, we calculated the averaged bulk Young's modulus and Poisson's ratio from our theoretical results of the elastic constants. These two elastic properties of bulk materials are needed in Eq. (9) to predict the Young's modulus of nanowires.

B. Surface materials

For fcc Ag and Au, the (111) surface has the lowest surface energy and thus is the most probable external surfaces of their nanostructures. For ZnO nanowires grown along [0001] direction, $(10\bar{1}0)$ and $(11\bar{2}0)$ surfaces are their lateral facets. Consequently, we conducted the DFT relaxation calculations for the (111) surface slab of fcc Ag (and Au) and $(10\bar{1}0)$ and $(11\bar{2}0)$ surface slabs of wurtzite ZnO. In our surface calculations, we used a surface slab (with two surfaces) having N_s layers of atoms in a periodic supercell which contains N_b atomic layers in the direction normal to the surface. To simulate the (111) surface of fcc Ag and Au, we used a supercell spanned with three orthogonal directions ([111], $[11\bar{2}]$ and $[1\bar{1}0]$). In the supercell (N_b=12), there are seven layer of atoms (N_s=7, about $2t$=14.4 Å thick of the Ag (111) slab and $2t$=14.5 Å thick of the Au (111) slab) and five layers of vacuum. For the (111) surface calculations, we used 8×12×2 k-point grid for k-space integration. For $(10\bar{1}0)$ surfaces, we used a supercell (N_b=16) containing eight atom layers (N_s=8, about $2t$=9.5 Å thick) and eight layers of vacuum. For $(11\bar{2}0)$ surface, we used a supercell (N_b=12) containing six atom layers (N_s=6, about $2t$=8.2 Å thick) and six layers of vacuum. For k-space integration, we used a 10×6×2 k-point grid for $(10\bar{1}0)$ surface and a 6×6×2 k-point grid for $(11\bar{2}0)$ surface.

Using slabs to simulate surfaces, we need conciliate two requirements: (a) the slab should be thin enough to represent two-dimensional surfaces and (b) the two surfaces of the slab should be separated far enough to minimize their interactions. In this work, we made our above choice of the thickness of the slabs by examining the separation of the layers in the slab after relaxation. For seven-layer Ag and Au (111) slab, the separation of the central layers differs by less than 0.2 % from the corresponding bulk value. For eight-

9

layer ZnO ($10\bar{1}0$) slab, the separation of the central layers differs by 5 % from the corresponding bulk value in contrast the separation of the outermost surface layers differs by 49.8 % from the corresponding bulk value. For six-layer ZnO ($11\bar{2}0$) slab, the separation of the central layers differs by 3 % from the corresponding bulk value while the separation of the outermost surface layers differs by 18.1 % from the corresponding bulk value. In this way, we attained a slab model whose central region is very close to the bulk materials and surface regions are subjected to the relaxation in vacuum.

Surface relaxation is quite insignificant for the (111) surfaces of Ag and Au. After geometry optimization, the outermost surface layer is found to move inward by 0.3 % of its bulk layer separation for Ag. This is close to the experimental measurement of about 0.0% relaxation of Ag(111) surface. [41] For Au, we found that the outermost surface layer moves outward by 1.2 % of its bulk layer separation. Prior DFT calculations also predicted an outward motion of the outermost layer of Au (111) surface. [42]

However, significant relaxation in both ($10\bar{1}0$) and ($11\bar{2}0$) surfaces of ZnO have been observed from our calculations. In bulk terminated ($10\bar{1}0$) and ($11\bar{2}0$) surfaces, Zn-O dimers lay in parallel to the surface. In contrast, the Zn-O dimers would tilt relative to the surface after relaxation. We found in our calculations that: in the outermost layer of ($10\bar{1}0$) surface, Zn cations move inward by $\Delta d_\perp$(Zn)= -0.34 Å and move laterally toward O by $\Delta d_\parallel$(Zn)= 0.16 Å, O anions move inward by $\Delta d_\perp$(O)= -0.002 Å, and the resultant tilt angle of Zn-O dimers to be ω= 10.6 °. Our results for the ($10\bar{1}0$) surface are in good agreement with the experimental data[43] ($\Delta d_\perp$(Zn)= -0.45±0.1 Å, $\Delta d_\parallel$(Zn)= 0.1±0.2 Å, $\Delta d_\perp$(O)= -0.05±0.1 Å, and ω=12°±5°). We also found in the outermost layer

of ($11\bar{2}0$) surface the tilt angle for Zn-O dimers to be 7.7 ° and a 6.1 % reduction of the Zn-O bond length, consistent with previous DFT results. [44]

Furthermore, we calculated the surface energy (γ) and surface stress tensor (g) for the relaxed Ag, Au, and ZnO surfaces using Eq. (10) as suggested in Ref. 45.

$$\gamma = \frac{1}{2A}[E_s - (N_s / N_b)E_b] \tag{10a}$$

$$g_{\alpha\beta} = \frac{1}{2A}[V\sigma_{\alpha\beta}^s - (N_s / N_b)V_b\sigma_{\alpha\beta}^b] \tag{10b}$$

where, A is the area on one side of the surface slab, E_s, V, and $\sigma_{\alpha\beta}^s$ are the energy, volume, and stress tensor for the supercell containing the relaxed surface slab, E_b, V_b, and $\sigma_{\alpha\beta}^b$ are the energy, volume, and stress tensor of the equilibrium bulk materials in the supercell.

To examine strain effect, we deformed the surfaces by a strain of ε, relaxed the surface slabs at each given strain, and calculated the corresponding surface energy and surface stress using Eq. (10). In Figure 1, we plot the calculated surface energies and surface stresses as a function of strain ε for Ag, Au, and ZnO. For Ag and Au, we deformed the (111) surfaces along both [$11\bar{2}$] and [$1\bar{1}0$] directions. For ZnO, we expanded the ($10\bar{1}0$) and ($11\bar{2}0$) surfaces along the [0001] direction.

Figure 1(a) shows that the surface energy of Ag (111) varies with the strain in a quadratic function form. The surface energy will have its minimum value at a strain of 0.3 % along [$11\bar{2}$] direction and a strain of -0.6 % along [$1\bar{1}0$] direction. Based on Eq. (3), the equilibrium strain in the Ag nanowires would be larger than -0.6 %. The surface stress exhibits a linear function of strain and is always positive when the strain in the

surface is larger than -0.7 %. Hence, surface stress will enhance (or stiffen) the Young's

modulus of Ag nanowires according to Eq. (9). It is noticeable in the lower panel of Fig.

1 that the calculated surface stresses along $[11\bar{2}]$ and $[1\bar{1}0]$ directions are not equal to

each other at the zero strain state of Ag (111) surface. This result is quite puzzling,

because the surface stress should be isotropic for the undeformed (111) surface of fcc

crystals owning to its three-fold rotational symmetry. [25] In some further tests, we found

that a non-negligible discrepancy in the calculated surface stress along the two directions

still exists even after we increase the k-points for integration, vary the number of surface

layers in our model, and/or switch to ultra-soft pseudopotential. Consequently, it appears

that there is some numerical error in determining surface stresses using DFT method.

However, our results (Fig. 3) will show that such errors in the values of calculated

surface stress do not have much effect on our model prediction of Young's modulus of

Ag nanowires.

Figure 1(b) for Au (111) surface indicates that the minimum of its surface energy will

be at a strain of -2.1 % along $[11\bar{2}]$ direction and a strain of -1.8 % along $[1\bar{1}0]$

direction. The surface stress would change from negative to positive at the strain of -2.9

% along the $[11\bar{2}]$ direction and the strain of -2.1 % along the $[1\bar{1}0]$ direction.

Conceivably, surface stress will enhance the Young's modulus for Au nanowires.

In stark contrast to the results of Ag and Au, it is seen in Fig. 1(c) for the two surfaces

of wurzite ZnO that the surface energies decrease with the expansion strain up to about

2.5 %, while the surface stresses (along [0001] direction) increase with the strain and

change signs (from negative to positive) at the strain about 1.25 %. Thus, our results in

Fig. 1(c) qualitatively point out that along [0001] direction the non-polar surfaces with a

strain below 1.25 % would facilitate elastic deformation and decrease (or soften) the elastic modulus of 1D ZnO nanomaterials.

C. Model predictions

Figures 1 (b) and (c) show clearly that the surfaces do not always have their minimum energy configuration at the state with a zero strain, where the bulk materials would reach their minimum energy. Thus, the surfaces will exert a contraction (for Au) or expansion (for ZnO) force on the whole nanowires. As a result, it is expected that the equilibrium Au nanowires are shorter than their bulk material counterparts and the equilibrium ZnO nanowires are longer than their bulk material counterparts. To quantify this equilibrium strain, we calculated the energy variations with the strains for bulk materials using DFT method. Then, we employed Eq. (3) to find the equilibrium strain (ε^*) for the nanowires with different diameters. We plotted the calculated equilibrium strain compared to the bulk lattice parameters in Fig. 2 for Ag, Au, and ZnO. Using the surface energies of ($10\bar{1}0$)/[0001] and ($11\bar{2}0$)/[0001] in Fig. 1(c), we predict an appreciable elongation (positive equilibrium strain) in the equilibrium ZnO nanowires; using the surface energies of (111)/[$11\bar{2}$] and (111)/[$1\bar{1}0$] in Fig. 1(b), we predict an appreciable contraction (negative equilibrium strain) in the equilibrium Au nanowires. However, we found in the equilibrium Ag nanowires a small positive strain using the surface energies of (111)/[$11\bar{2}$] (Fig. 1(a)) but a small negative strain using the surface energies of (111)/[$1\bar{1}0$] (Fig. 1(a)).

Through first-principles calculations, we have determined the value of bulk Young's modulus (E_b), Poisson's ratio (ν), equilibrium strain (ε^*), and surface stress (g) as a

function of strain. In this work, we assume L=1000 nm, which is the typical suspended length of the nanowires in atomic force microscopy three-point bending tests. Inputting all those calculated material-dependent parameters into Eq. (9), we predict the Young's modulus of the nanowires for Ag (Fig. 3), Au (Fig. 4), and ZnO (Fig. 5) as a function of their diameters.

In Fig. 3, we predict that the Young's modulus of Ag nanowire increases when its diameter decreases. This is because Ag (111) surfaces have a positive surface stress and thus enhance the Young's modulus of the nanowires. Moreover, our theoretical predictions (lines) agree excellently with experimental measurement data (circles) in Fig. 3. Moreover, our model predicts in Fig. 4 that the Young's modulus of Au nanowire would also increase when its diameter decreases due to its positive surface stress. Although it was believed that the Young's modulus of Au nanowires is "independent" of diameter in Ref. 7, Fig. 4 shows that the same experimental data (especially the data for the Au nanowires with diameters around 50 nm) are actually consistent with our model of enhancing Young's modulus for Au nanowires.

It is worth mentioning that the increase of the Young's modulus with the decreasing diameter of Au nanowires is quite slow when the nanowire diameters are larger than 75 nm. The calculated Young's modulus of the Au nanowire with a diameter of 75 nm is only about 9 % higher than the bulk Young's modulus of Au. This apparent "independency" is a result of two effects: (1) a compressive (negative) equilibrium strain in the nanowire core leads to a decrease of the Young's modulus of the nanowires, and (2) a positive surface stress in the nanowire surface leads to an increase of the Young's modulus of the nanowires. When the diameter of Au nanowires are small (less than 75

nm), surface stress effect becomes dominant and is responsible for the sharp increase of the Young's modulus as shown in Fig. 4.

Plotted in Fig. 5 for ZnO nanowires with D>20 nm, our model predicts a decrease in their Young's modulus when reducing their diameters. This is due to the negative surface stress of ZnO surfaces (see Fig. 1(c)). At this moment, there are no available (three-point bending) experimental data of the Young's modulus of ZnO nanowires for us to directly compare our theoretical predictions with. However, there is much experimental evidence that ZnO nanostructures have a lower elastic modulus than ZnO bulk materials. [8-13] Thus, our model prediction in Fig. 5 is qualitatively consistent with those measurements. We also notice that some studies report that ZnO nanowires have higher Young's modulus that increases with the decreasing size. [14,15] Here, we postulate an explanation to this discrepancy in the literature. Our results in Figs. 1(c) and 5 are obtained from the fully-relaxed ZnO surfaces, which are quite different from the corresponding bulk terminated surfaces (see details in Sec. III.B). We found from our calculations for ZnO that the surface stresses are negative for the fully-relaxed surfaces but positive for the un-relaxed bulk terminated surfaces. This suggests that the value (positive or negative) of surface stress may strongly depend on the extent of the surface relaxation process. Surface relaxation process can be changed by surface contamination or surface charges, [46] which can be introduced during sample preparation and measurement process. Thus, the Young's modulus of ZnO nanowires with a same diameter might exhibit different values due to the surface stress effect for various surface conditions of the experimental samples.

Although our model (Eq. (9)) leads to satisfactory agreement between the theoretical and experimental data for nanowires with a diameter larger than 20 nm, some further

improvement is required to accurately predict the Young's modulus of small nanowires with a diameter below 20 nm. For example, we express the total energy of nanowires as a linear combination of its bulk and surface contribution in Eq. (1). When the nanowires have very small diameters, some non-linear term must be included to that equation. In addition, we currently use a flat, extended surface slab to model the nanowire surfaces. For small nanowires, their surfaces are highly curved and hence have a significant transverse stress (strain) component. Thus, the curvature effect must also be properly addressed in an elaborated model for small nanowires.

IV. CONCLUSIONS

In this work, we first developed a model to predict the Young's modulus of nanowires from the properties of the corresponding bulk and surface materials. We included two effects (equilibrium strain and surface stress) in our model to account for the geometric size influence on the elastic properties of nanowires. To accurately describe the surface stress effect, we must know the exact deformation process of nanowires. This is because different loading conditions (for example, axial tensile test and three-point bending test) would lead to different values of the changes in the length and surface area of the nanowires during the elastic deformation. For a direct comparison to experimental data, we focus on studying the clamped-end three-point bending loading condition.

Furthermore, we calculated the bulk and surface properties of the materials using first-principles DFT method. The calculated properties include Young's modulus, Poisson's ratio, surface energy, and surface stress. Taking those theoretical data as inputs, we predicted the Young's modulus of Ag, Au, and ZnO nanowires as a function of

nanowire diameter. To validate our model and approach, we compared our theoretical results with the experiment measurement results. It is found that our model predictions for Ag and Au nanowires agree excellently with those experimental data. For ZnO nanowires with D>20 nm, our predictions also agree qualitatively with a series of experimental results. We believe that the agreement between our model and experimental data is remarkable since we did not introduce any empirical data modifications in our theoretical approach.

Our model reveals two major effects that the surface exerts on the elastic deformation process of nanomaterials. First, the surface may have different minimum-energy lattice parameters than the bulk lattice parameters of the material and thus result an equilibrium strain in the nanowire core region. Second, the surface may have tensile or compressive surface stress that is the energy required to elastically deform the surface. A tensile surface stress would lead to an increase in Young's modulus with the decreasing size of nanowires, while a compressive surface stress would lead to a decrease in Young's modulus with the decreasing size of nanowires.

Our model indicates that the tensile (positive) surface stress is the reason for Ag and Au nanowires showing an enhanced Young's modulus when reducing nanowire diameters. This viewpoint has been accepted owning to the support of myriads of experimental and simulation studies. [4,7,25] Our model also points out that the compressive (negative) surface stress in ZnO nanowires (with D> 20 nm) would lead to a softened Young's modulus when reducing nanowire diameters. We notice that some other materials, such as Si, [6] GaN, [47-49] and ZnS, [50,51] exhibit the reduced Young's modulus when decreasing the size of their nanomaterials. Hence, we proposed based on our results

that the compressive surface stress, which is an inherent material property, is responsible for the observed lower Young's modulus of those nanomaterials compared to their bulk modulus.

Since surface stress plays a very important role in determining the Young's modulus of nanomaterials, it is reasonable to expect that the elastic properties of nanomaterials could be engineered by altering the surface stress through rational control of the adsorptions, charges, structure, and impurities in the surfaces.

References:

1. K.L. Ekinci and M.L. Roukes, Rev. Sci. Instrum. **76**, 061101 (2005).

2. X. Wang, J. Song, J. Liu, and Z.L. Wang, Science **316**, 102 (2007).

3. S. Cuenot, C. Frétigny, S. Demoustier-Champagne, and B. Nysten, Phys. Rev. B **69**, 165410 (2004).

4. G.Y. Jing, H.L. Duan, X.M. Sun, Z.S. Zhang, J. Xu, Y.D. Li, J.X. Wang, and D.P. Yu, Phys. Rev. B **73**, 235409 (2006).

5. X. Li, T. Ono, Y. Wang, and M. Esashi, Appl. Phys. Lett. **83**, 3081 (2003).

6. S.G. Nilsson, X. Borrisé, and L. Montelius, Appl. Phys. Lett. **85**, 3555 (2004).

7. B. Wu, A. Heidelberg, and J.J. Boland, Nature Mater. **4**, 525 (2005).

8. X.D. Bai, P.X. Gao, Z.L. Wang, and E.G. Wang, Appl. Phys. Lett. **82**, 4806 (2003).

9. J. Song, X. Wang, E. Riedo, and Z.L. Wang, Nano Lett. **5**, 1954 (2005).

10. M.H. Zhao, C.B. Jiang, S.X. Li, and S.X. Mao, Mater. Sci Eng. A **409**, 223 (2005).

11. H. Ni and X.D. Li, Nanotechnology **17**, 3591 (2006).

12. W. Mai and Z.L. Wang, Appl. Phys. Lett. **89**, 073112 (2006).

13. M. Lucas, W. Mai, R. Yang, Z.L. Wang, and E. Reido, Nano Lett. **7**, 1314 (2007).

14. C.Q. Chen, Y. Shi, Y.S. Zhang, J. Zhu, and Y.J. Yan, Phys. Rev. Lett. **96**, 075505 (2006).

15. G. Stan, C.V. Ciobanu, P.M. Parthangal, and R.F. Cook, Nano Lett. 7, 3691 (2007).

16. J. Q. Broughton, C. A. Meli, P. Vashishta, and R. K. Kalia, Phys. Rev. B **56**, 611 (1997).

17. R. E. Miller and V. B. Shenoy, Nanotechnology, **11**, 139 (2000).

18. V. B. Shenoy, Phys. Rev. B **71**, 094104 (2005).

19. L. G. Zhou and H. C. Huang, Appl. Phys. Lett. **84**, 1940 (2004).

20. H. Y. Liang, M. Upmanyu, and H. C. Huang, Phys. Rev. B **71**, 241403 (2005).

21. R. C. Cammarata, Prog. Surf. Sci. **1**, 1 (1994).

22. G. Wang and X.D. Li, Appl. Phys. Lett. **91**, 231912 (2007).

23. H.S. Park, J. Appl. Phys. **103**, 123504 (2008).

24. W. Zhang, T. Wang, and X. Chen, J. Appl. Phys. **103**, 123527 (2008).

25. J. Diao, k. Gall, and M.L. Dunn, J. Mech. Phys. Solids **52**, 1935 (2004).

26. B. Lee and R.E. Rudd, Phys. Rev. B **75**, 041305(R) (2007).

27. J.M. Gere and S.P. Timoshenko, *Mechanics of Materials* (PWS Engineering, Boston, 1987), p. 434.

28. G. Kresse and J. Hafner, Phys. Rev. B **47**, 558 (1993).

29. G. Kresse and J. Furthmüller, Phys. Rev. B **54**, 11169 (1996).

30. G. Kresse and D. Joubert, Phys. Rev. B **59**, 1758 (1999).

31. J.P. Perdew and Y. Wang, Phys. Rev. B **45**, 13244 (1992).

32. P. Söderlind, O. Eriksson, J.M. Wills, and A.M. Boring, Phys. Rev. B **48**, 5844 (1993).

33. L. Fast, J.M. Wills, B. Johansson, and O. Eriksson, Phys. Rev. B **51**, 17431 (1995).

34. N.W. Ashcroft and N.D. Mermin, *Solid State Physics* (Holt, Rinehart and Winston, New York, 1976).

35. G. Simmons and H. Wang, *Single Crystal Elastic Constants and Calculated Aggregate Properties: A Handbook* (MIT Press, Cambridge, 1971).

36. H. Rolnick, Phys. Rev. **36**, 506 (1930).

37. H. Karzel, W. Potzel, M. Köfferlein, W. Schiessl, M. Steiner, U. Hiller, G.M. Kalvius, D.W. Mitchell, T.P. Das, P. Blaha, K. Schwarz, and M.P. Pasternak, Phys. Rev. B **53**, 11425 (1996).

38. J. Albertsson, S.C. Abrahams, and Å. Kvick, Acta Crystallogr. B **45**, 34 (1989).

39. T.B. Bateman, J. Appl. Phys. **33**, 3309 (1962).

40. S.O. Kucheyev, J.E. Bradby, J.S. Williams, C. Jagadish, and M.V. Swain, Appl. Phys. Lett. **80**, 956 (2002).

41. F. Soria, J.L. Sacedon, P.M. Echenigire, and D. Titherington, Surf. Sci. **68**, 448 (1977).

42. Ž. Crljen, P. Lazić, D. Šokčević, and R, Brako, Phys. Rev. B **68**, 195411 (2003).

43. C.B. Duke, R.J. Meyer, A. Paton, and P. Mark, Phys. Rev. B **18**, 4225 (1978).

44. B. Meyer and D. Marx, Phys. Rev. B **67**, 035403 (2003).

45. R.J. Needs, Phys. Rev. Lett. **58**, 53 (1987).

46. G.A. Somorjai, Annu. Rev. Phys. Chem. **45**, 721 (1994).

47. C.Y. Nam, P. Jaroenapibal, D. Tham, D.E. Luzzi, S. Evoy, and J.E. Fischer, Nano Lett. **6**, 153 (2006).

48. H. Ni, X. D. Li, G. S. Cheng, and R. Klie, J. Mater. Res. **21**, 2882 (2006).

49. G. Feng, W.D. Nix, Y. Yoon, and C.J. Lee, J. Appl. Phys. **99**, 074304 (2006).

50. X. D. Li, X.X. Wang, Q.H. Xiong, and P.C. Eklund, Nano Lett. **5**, 1982 (2005).

51. Q. Xiong, N. Duarte, S. Tadigadapa, and P.C. Eklund, Nano Lett. **5**, 1904 (2006).

Table:

TABLE I. Calculated equilibrium lattice constants (*a*), elastic constants (C_{11}, C_{12}, and C_{44}), Young's modulus (*E*), and Poisson's ratio (ν) of fcc Ag and Au using first-principles DFT method. For comparison, the experimental values are also given.

	Ag		Au	
	This work	Exp.	This work	Exp.
a (Å)	4.159	4.09 [a]	4.174	4.08 [a]
C_{11} (GPa)	117.7	124 [b]	165.9	186 [b]
C_{12} (GPa)	90.3	93.4 [b]	142.2	157 [b]
C_{44} (GPa)	38.0	46.1 [b]	26.7	42 [b]
E (GPa)	77.5 [c]	79 [e]	59.5 [c]	80 [e]
ν	0.370 [d]	0.38 [e]	0.434 [d]	0.42 [e]

[a] Reference 34.

[b] Reference 35.

[c] $$E = \frac{(C_{11} - C_{12} + 3C_{44})(C_{11} + 2C_{12})}{2C_{11} + 3C_{12} + C_{44}}$$

[d] $$\nu = \frac{5(C_{11} + 2C_{12})}{2(2C_{11} + 3C_{12} + C_{44})} - 1$$

[e] Reference 36.

TABLE II. Calculated equilibrium lattice constants (*a* and *c*), internal parameter (*u*), elastic constants (C_{11}, C_{12}, C_{13}, C_{33}, and C_{55}), Young's modulus (*E*), and Poisson's ratio (ν) of wurtzite ZnO using first-principles DFT method. For comparison, the experimental values are also given.

	This work	Exp.
a (Å)	3.282	3.2496 [a]
c (Å)	5.292	5.2042 [a]
u	0.380	0.3819 [b]
C_{11} (GPa)	191.7	209.7 [c]
C_{12} (GPa)	110.0	121.1 [c]
C_{13} (GPa)	96.7	105.1 [c]
C_{33} (GPa)	203.4	210.9 [c]
C_{55} (GPa)	37.2	42.5 [c]
E (GPa)	113.8 [d]	111.2 [e]
ν	0.357 [d]	-

[a] Reference 37.

[b] Reference 38.

[c] Reference 39.

[d] $E = \dfrac{(F - G + 3H)(F + 2G)}{2F + 3G + H}$ and $v = \dfrac{5(F + 2G)}{2(2F + 3G + H)} - 1$

here, $F = \dfrac{2C_{11} + C_{33}}{3}$, $G = \dfrac{C_{12} + 2C_{13}}{3}$, and $H = \dfrac{4C_{44} + C_{11} - C_{12}}{6}$

[e] Reference 40.

Figure Captions:

Figure 1. Variation of the surface energies (γ) and the surface stresses (g) along (a) the $[11\bar{2}]$ and $[1\bar{1}0]$ directions of Ag (111) surface, (b) the $[11\bar{2}]$ and $[1\bar{1}0]$ directions of Au (111) surface, and (c) the [0001] direction of ZnO ($10\bar{1}0$) and ($11\bar{2}0$) surfaces. In the figures, the dashed lines in the upper panel are the quadratic function fitting of calculated surface energy data and the dashed lines in the lower panel are the linear fitting of calculated surface stress data.

Figure 2. Calculated equilibrium strains in the equilibrium Ag, Au, and ZnO nanowires as a function of nanowire diameter.

Figure 3. Size dependency of the Young's modulus of Ag nanowires enclosed by (111) surfaces. The solid line and dashed line show the model predictions using the surface properties of (111)/$[11\bar{2}]$ and (111)/$[1\bar{1}0]$, respectively. For comparison, the experimental data from Ref. 4 are plotted as circles.

Figure 4. Size dependency of the Young's modulus of Au nanowires enclosed by (111) surfaces. The two dashed lines (overlapped with each other) show the model predictions using the surface properties of (111)/$[11\bar{2}]$ and (111)/ $[1\bar{1}0]$. For comparison, the experimental data from Ref. 7 are plotted as circles.

Figure 5. Predicted size dependency of the Young's modulus of ZnO nanowires enclosed by ($10\bar{1}0$) surfaces (solid line) or ($11\bar{2}0$) surfaces (dashed line).
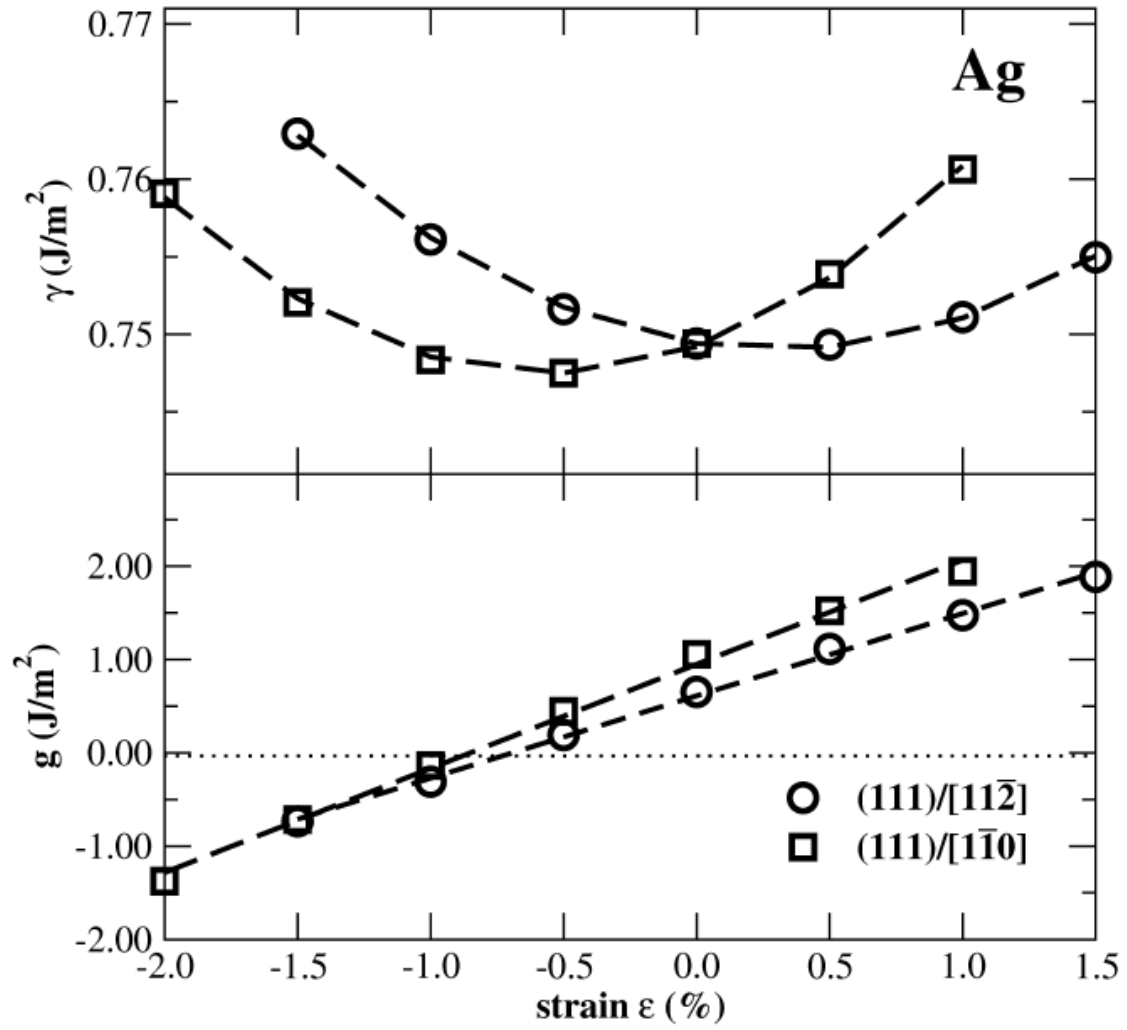
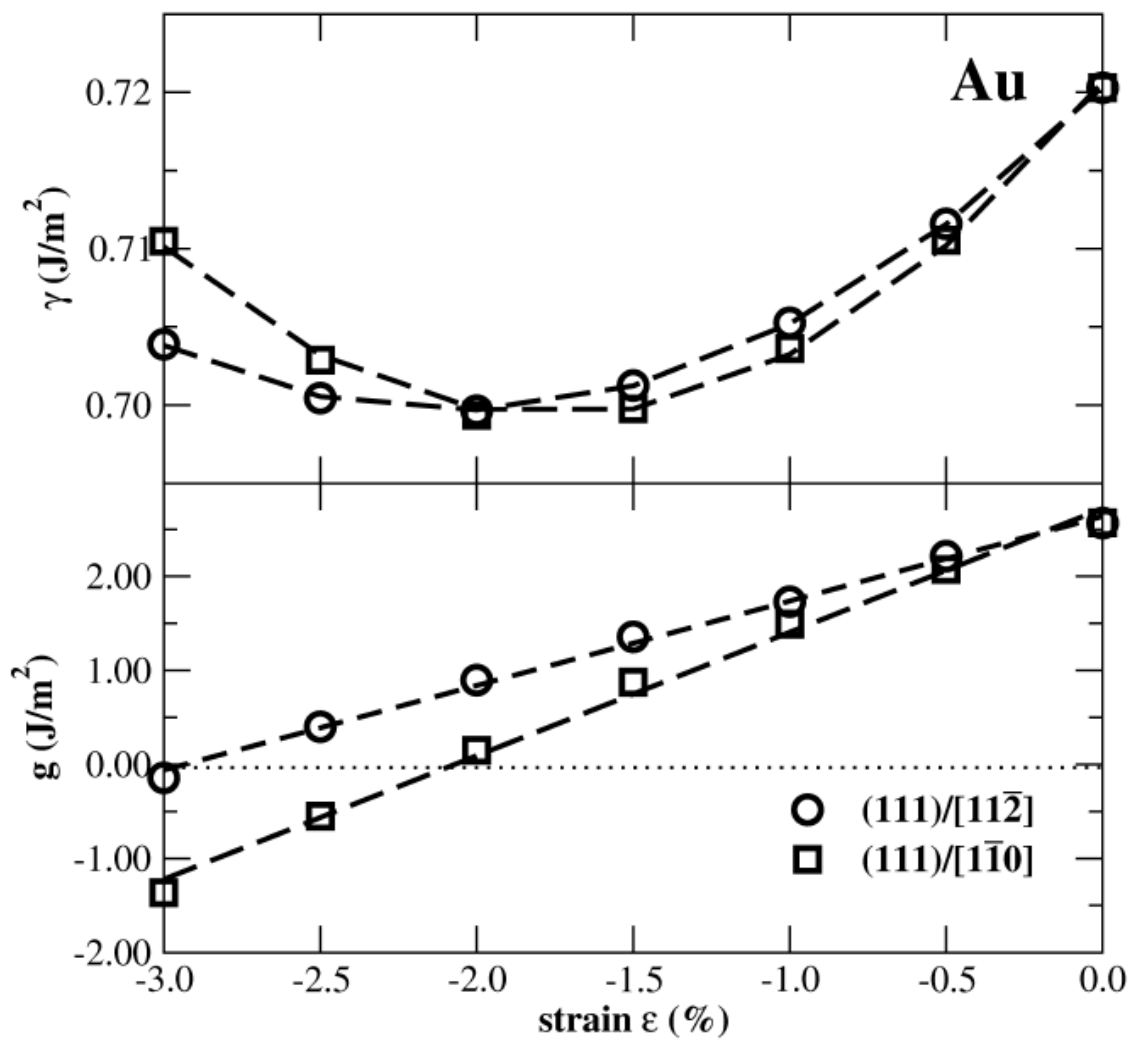Figure 1(a). G. Wang et al

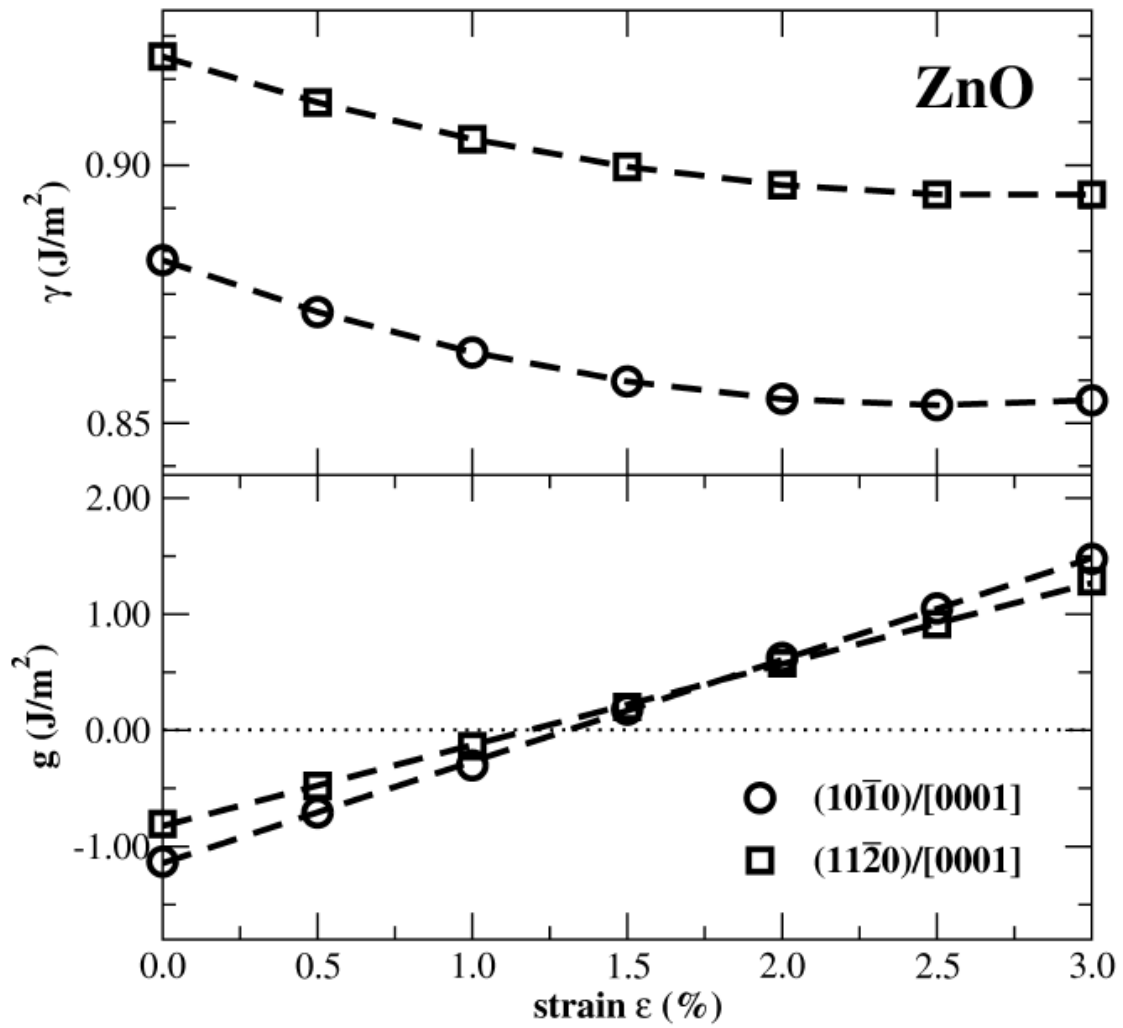# Figure 1(b). G. Wang et al

Figure 1(c). G. Wang et al

ZnO

Fig. 2. G. Wang et al

The figure shows Equilibrium Strain (%) versus D (nm).

line 1: ZnO, $(10\bar{1}0)/[0001]$
line 2: ZnO, $(11\bar{2}0)/[0001]$
line 3: Ag, $(111)/[11\bar{2}]$
line 4: Ag, $(111)/[1\bar{1}0]$
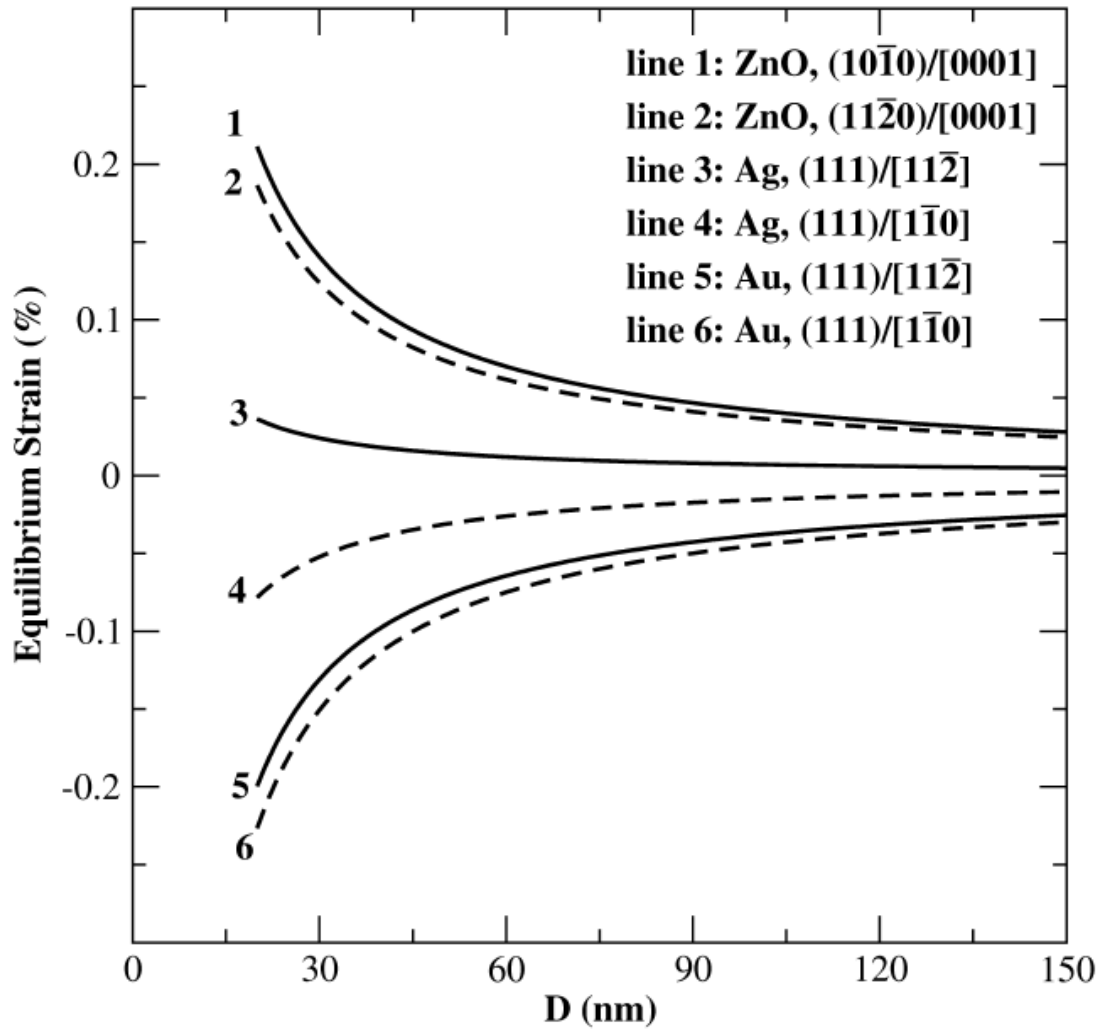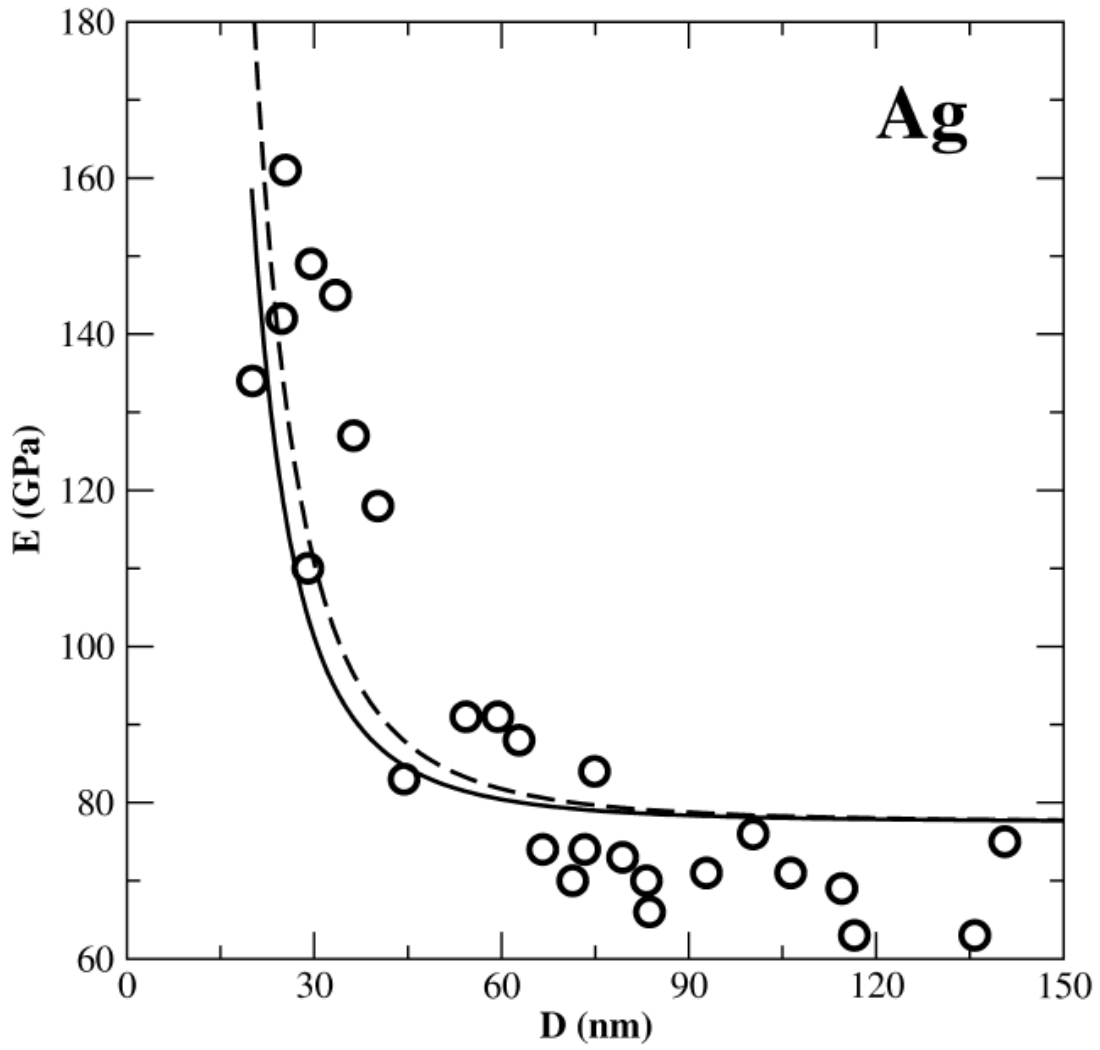line 5: Au, $(111)/[11\bar{2}]$
line 6: Au, $(111)/[1\bar{1}0]$

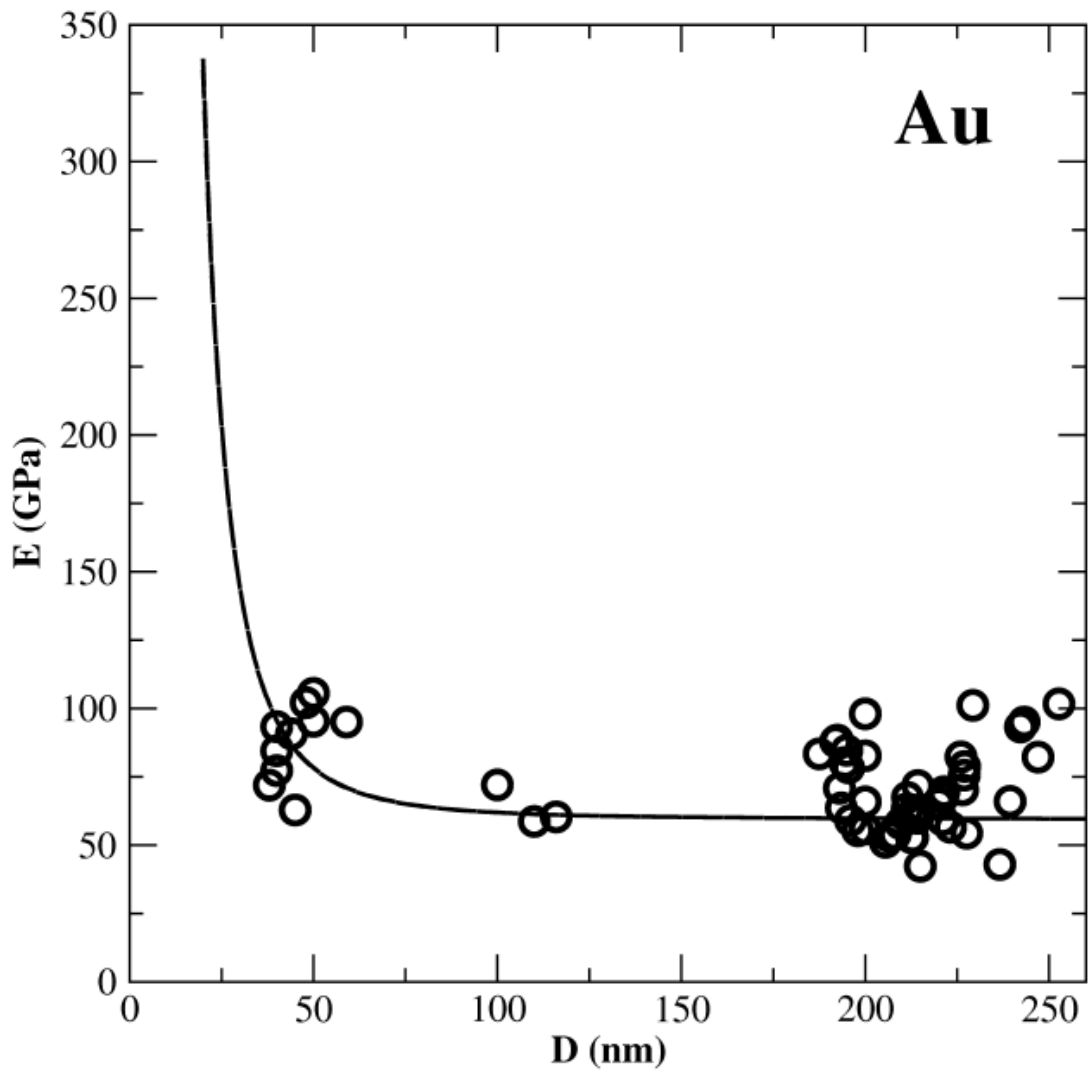Fig 3. G. Wang et al

Fig 4. G. Wang et al

Fig 5. G. Wang et al

ZnO